

Supporting Information

Biomimetic oxygen reduction by cofacial porphyrins at a liquid-liquid interface

Pekka Peljo^a, Lasse Murtomäki^{a,*}, Tanja Kallio^a, Hai-Jun Xu^b, Michel Meyer^b, Claude P. Gros^b, Jean-Michel Barbe^b, Hubert H. Girault^c, Kari Laasonen^a and Kyösti Kontturi^a

^a Aalto University, Department of Chemistry, P.O. Box 16100, 00076 Aalto, Finland

^b Institut de Chimie Moléculaire de l'Université de Bourgogne (ICMUB), UMR CNRS 6302, 9 avenue A. Savary, BP 47870, 21078 Dijon Cedex, France

^c Laboratoire d'Electrochimie Physique et Analytique, Ecole Polytechnique Fédérale de Lausanne (EPFL), Station 6, CH-1015 Lausanne, Switzerland

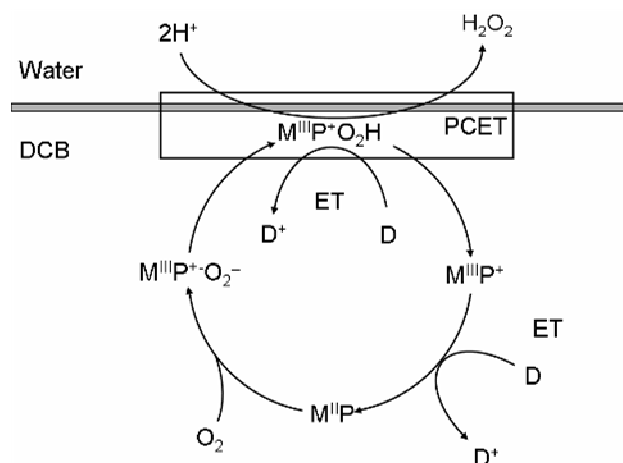
*Corresponding author

Tel. +358 9 470 22575

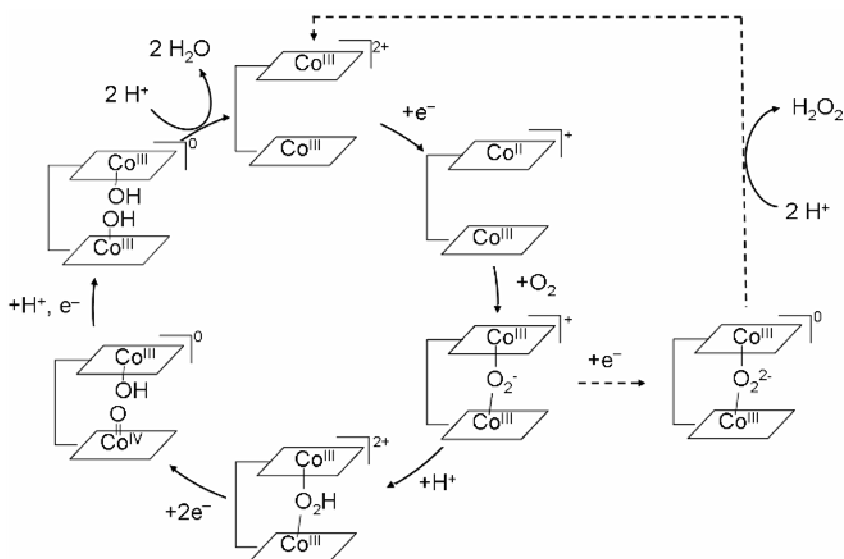
Fax +358 9 470 22580

Email lasse.murtomaki@aalto.fi

1 Reaction schemes of oxygen reduction reported previously



Scheme S-1. Reaction scheme for oxygen reduction by a mediator catalyzed by metal porphyrins. IT stands for ion transfer and ET for electron transfer, adapted from ref. s1.



Scheme S-2. Reaction scheme for oxygen reduction by a mediator catalyzed by cofacial metal bisporphyrin, adapted from ref. s2.

2 Electrochemical measurements

Figure S-1 shows the voltammetry of 100 μM catalyst + 5 mM BATB in DCB for various proton concentrations in the aqueous phase. A dependence of the transfer potentials of chloride and protons of ca. 60 mV vs. $\log [\text{HCl}]$ is observed. Also, a wave for facilitated transfer of chloride is observed at 0.0 V (pH = 0) for $\text{Co}_2(\text{DPX})$ and $\text{Co}_2(\text{DPOx})$, as this wave shifts to more positive potentials with increasing chloride concentration (also ca. 60 mV vs. $\log [\text{HCl}]$). No significant adsorption on the interface is observed, as the capacitance remains virtually unchanged.

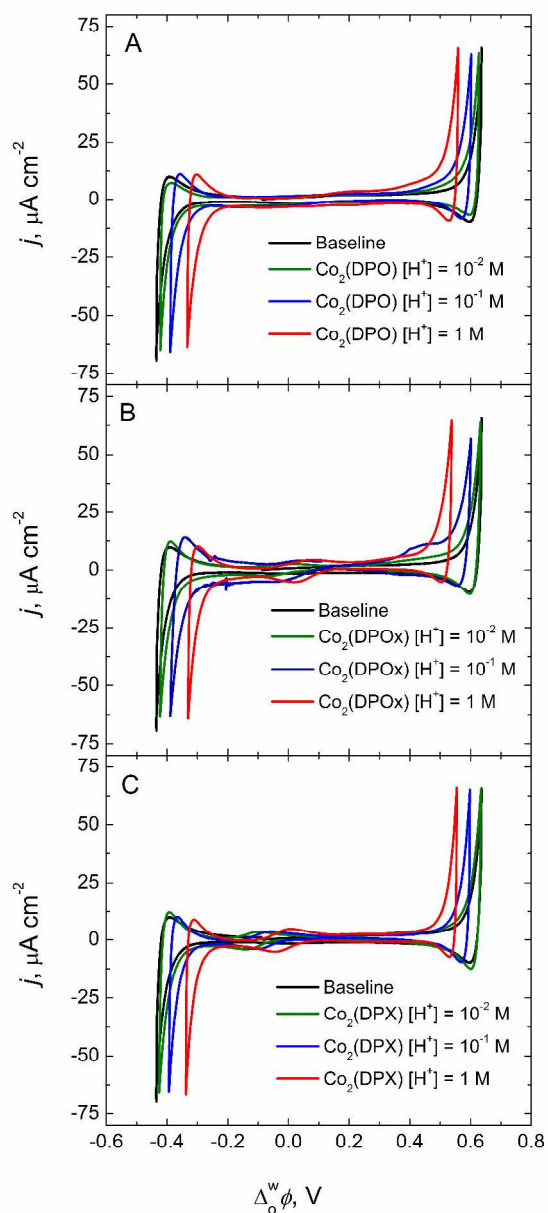


Figure S-1. Cyclic voltammograms of 100 μM $\text{Co}_2(\text{DPO})$ (A), $\text{Co}_2(\text{DPOx})$ (B) and $\text{Co}_2(\text{DPX})$ (C) with 5 mM BATB in DCB for various proton concentrations in the aqueous phase. The baseline corresponds to the CV of 5 mM BATB in DCB in contact with 10 mM aqueous HCl.

3 UV-Vis measurements

Figure S-2 shows UV-Vis spectra of DCB phases before and after 30 s biphasic reaction. DMFc has a peak at 439 nm and DMFc^+ has a broad peak at 550-725 nm, so it is clearly seen from Figure S-2 that oxygen reduction takes place and DMFc^+ is formed during the reaction.

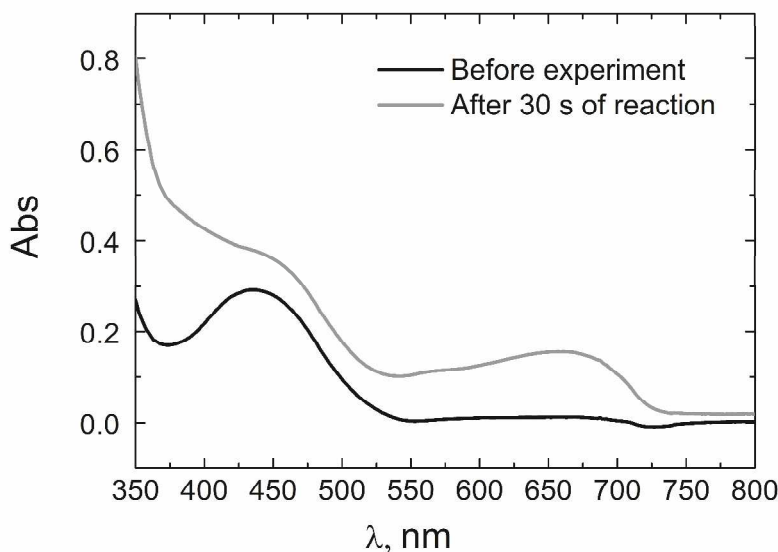


Figure S-2. UV-Vis spectra of DCB phases containing 2 mM DMFc and 5 mM BATB before and after 30 s two-phase reaction (25% conversion), showing a broad peak of DMFc^+ in the 550-725 nm range.

The comparison of UV-Vis spectra of the DCB phase (100 μM $\text{Co}_2(\text{DPOx}) + 2$ mM DMFc + 5 mM BATB) after oxygen reduction in aerobic conditions (5 mM LiTB + 10 mM HCl in aqueous phase) and biphasic reaction with hydrogen peroxide in anaerobic

conditions (1 mM H₂O₂ + 5 mM LiTB + 10 mM HCl in aqueous phase) after 60 s of reaction are shown in Figure S-3. DMFc⁺ is observed in both cases ($\lambda = 550-725$ nm), indicating that hydrogen peroxide reduction is catalyzed by cofacial porphyrins.

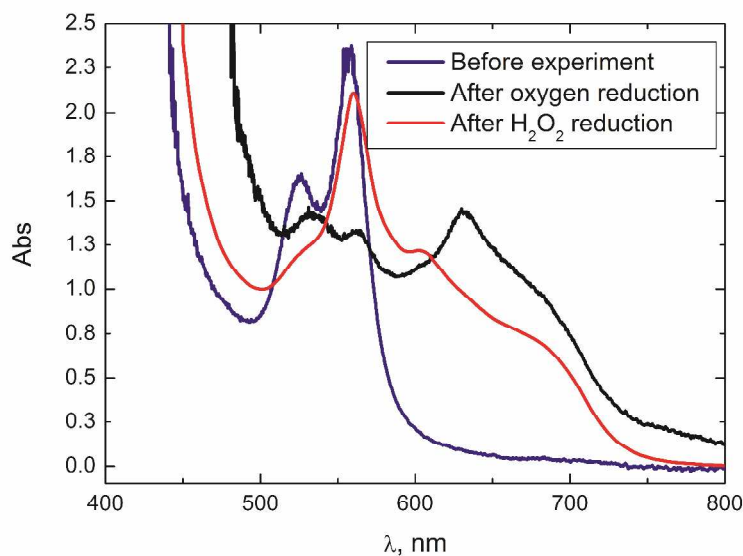


Figure S-3. Comparison of UV-Vis spectra of a 2 mM DMFc and 100 μM Co₂(DPO_x) solution in DCB before and after oxygen reduction in biphasic experiment and after hydrogen peroxide reduction in anaerobic conditions in biphasic experiment.

4 Calculation of the Galvani potential difference across the liquid-liquid interface

In a system where ionic species of the two immiscible liquid phases are in equilibrium, the potential difference across the interface can be calculated with the Nernst equation.^{s3}

$$\Delta_o^w \phi = \Delta_o^w \phi_i^0 + \frac{RT}{z_i F} \ln \frac{c_i^o}{c_i^w} \quad (\text{SI 1})$$

The mass balance for the species i is

$$n_{i, \text{total}} = n_i^o + n_i^w \quad (\text{SI 2})$$

$$V_o c_{i, \text{initial}}^o + V_w c_{i, \text{initial}}^w = V_o c_i^o + V_w c_i^w \quad (\text{SI 3})$$

Additionally, electroneutrality condition of the both phases must be fulfilled:

$$\sum_i z_i c_i^w = \sum_i z_i c_i^o = 0 \quad (\text{SI 4})$$

In a case where $V_o = V_w$ combination of the equations (SI 1-4) gives

$$\sum_i z_i \frac{c_{i, \text{total}}}{1 + \exp\left[\frac{z_i F}{RT} (\Delta_o^w \phi - \Delta_o^w \phi_i^0)\right]} = 0 \quad (\text{SI 5})$$

Solution of the equation (SI 5) gives the Galvani potential difference of the system in equilibrium, and Nernst equation and mass balance equations can be used to calculate the compositions of both phases, as shown in Table S-1. The Gibbs transfer energies of the species were estimated as described in the Supporting Information of ref. s4.

Table S-1. Calculated equilibrium concentrations (mM) between 5 mM BATB in DCB and 10 mM HCl and 5 mM LiTB in water in the beginning and in the end of the reaction corresponding to full conversion of the 2 mM DMFc to DMFc⁺.

	Beginning		End	
	water	DCB	water	DCB
BA ⁺	2.77×10^{-22}	5.00	5.23×10^{-22}	5.00
TB [□]	3.82	6.18	2.47	7.53
H ⁺	8.9	1.14	7.49	0.51
Li ⁺	4.96	0.04	4.98	0.02
Cl [□]	10.00	2.40×10^{-15}	10.00	4.52×10^{-15}
DMFc ⁺	-	-	1.13×10^{-11}	2.00

5 Standard redox potentials of hydrogen evolution and oxygen reduction in benzonitrile

The standard redox potentials of the reactions in benzonitrile can be estimated with the thermodynamic cycle.^{s5} In general, the reduction of O to R in phase α is expressed as:



where the standard redox potential can be expressed as^{s6}

$$\left[E_{O/R}^0 \right]_{\text{SHE}}^\alpha = -\frac{\Delta G^0}{nF} = \frac{1}{nF} \left(\mu_{\text{O}}^{\circ,\alpha} - \mu_{\text{R}}^{\circ,\alpha} - n \left(\mu_{\text{H}^+}^{\circ,\text{w}} - \frac{1}{2} \mu_{\text{H}_2}^{\circ,\text{w}} \right) \right) \quad (\text{SI } 7)$$

So, the standard redox potentials of the reaction (SI 6) in benzonitrile and aqueous phase are

$$\left[E_{O/R}^0 \right]_{SHE}^{BCN} = \frac{1}{nF} \left(\mu_{O}^{\circ,BCN} - \mu_{R}^{\circ,BCN} - n \left(\mu_{H^+}^{\circ,w} - \frac{1}{2} \mu_{H_2}^{\circ,w} \right) \right) \quad (SI 8)$$

$$\left[E_{O/R}^0 \right]_{SHE}^w = \frac{1}{nF} \left(\mu_{O}^{\circ,w} - \mu_{R}^{\circ,w} - n \left(\mu_{H^+}^{\circ,w} - \frac{1}{2} \mu_{H_2}^{\circ,w} \right) \right) \quad (SI 9)$$

When eq. (SI 8) is subtracted from eq. (SI 9), eq. (SI 10) is obtained:

$$\begin{aligned} \left[E_{O/R}^0 \right]_{SHE}^{BCN} - \left[E_{O/R}^0 \right]_{SHE}^w &= \frac{1}{nF} (\mu_{O}^{\circ,BCN} - \mu_{R}^{\circ,BCN} - \mu_{O}^{\circ,w} + \mu_{R}^{\circ,w}) = \\ &= \frac{1}{nF} (\Delta_o^w G_R^0 - \Delta_o^w G_O^0) \end{aligned} \quad (SI 10)$$

where $\Delta_o^w G_i^0$ is the Gibbs energy of transfer of the species i from oil phase to aqueous phase. Standard redox potentials of the following reactions in BCN were calculated with eq. (SI 10).



$$\left[E_{H^+/H_2}^0 \right]_{SHE}^{BCN} = \left[E_{H^+/H_2}^0 \right]_{SHE}^w + \frac{1}{F} (\Delta_o^w G_{H_2}^0 - \Delta_o^w G_{H^+}^0) \quad (SI 14)$$

$$\left[E_{O_2/H_2O_2}^0 \right]_{SHE}^{BCN} = \left[E_{O_2/H_2O_2}^0 \right]_{SHE}^w + \frac{1}{2F} (\Delta_o^w G_{H_2O_2}^0 - \Delta_o^w G_{O_2}^0 - 2\Delta_o^w G_{H^+}^0) \quad (SI 15)$$

$$\left[E_{O_2/H_2O}^0 \right]_{SHE}^{BCN} = \left[E_{O_2/H_2O}^0 \right]_{SHE}^w + \frac{1}{2F} (\Delta_o^w G_{H_2O}^0 - 1/2 \Delta_o^w G_{O_2}^0 - 2\Delta_o^w G_{H^+}^0) \quad (SI 16)$$

In benzonitrile, $\Delta_o^w G_{H^+}^0 = 33 \text{ kJ / mol}$,^{s7} and $\Delta_o^w G_{H_2O}^0$ was calculated from the solubility data (the solubility of water to BCN is about 1.21 w/w % = 0.67 mol dm⁻³)^{s8} and

$\Delta_o^w G_{\text{H}_2\text{O}_2}^0$ was estimated to be close to the value for $\Delta_o^w G_{\text{H}_2\text{O}}^0$. Transfer energies of gasses were considered to have little effect on the standard redox potential. Results are shown in Table S-2.

Table S-2. Standard redox potentials of hydrogen evolution and oxygen reduction reactions in BCN.

Reaction	E^0 vs. SHE in BCN (V)
$\text{H}^+ + \text{e}^- \rightleftharpoons 1/2 \text{H}_2$	0.34
$\text{O}_2 + 2 \text{H}^+ + 2 \text{e}^- \rightleftharpoons \text{H}_2\text{O}_2$	0.98
$1/2 \text{O}_2 + 2 \text{H}^+ + 2 \text{e}^- \rightleftharpoons \text{H}_2\text{O}$	1.53

8 Estimation of the rate constants

The rate of reaction was assumed to be first order in respect to DMFc, as the same reaction order has been found for the hydrogen evolution by DcMFC catalyzed by MoS₂ nanoparticles at a liquid-liquid interface.^{s9} Both oxygen reduction and hydrogen evolution are similar proton-coupled electron transfer reactions, and thus can be treated in the same way as a first assumption. Therefore, the reaction rate can be written as

$$v = \frac{d[\text{D}^+]}{dt} = k_{\text{app}}[\text{D}] \quad (\text{SI } 17)$$

where k_{app} is the apparent rate constant of the reaction. The integrated rate law was expressed as^{s10}

$$k_{\text{app}}t = \ln \frac{a}{a-x} \quad (\text{SI 18})$$

where a is the initial concentration of the electron donor and x is the concentration of D^+ . The right hand side of eq. (SI 18) when plotted as a function of time gives a straight line with a slope of k_{app} . The catalyzed reactions finished in less than 1 minute, so the minimum value for the rate constant was estimated by assuming that 1% of the reactant was unreacted at the end of the reaction. The data is presented in Figure S-4, and in Table 2.

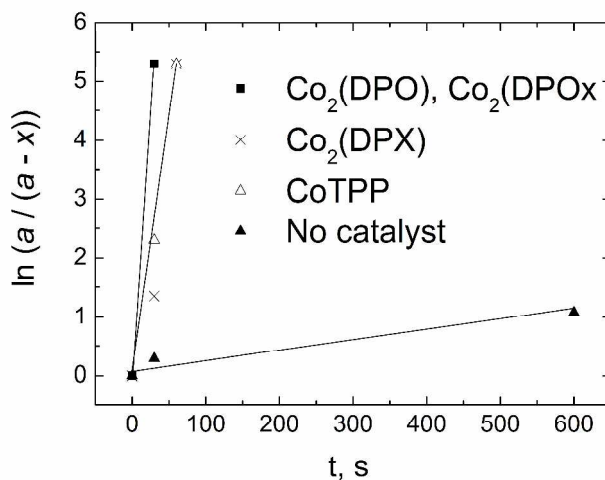


Figure S-4. Plot of the integrated rate law (SI-18) for the estimation of the minimum value of the rate constant. a is the initial concentration of DMFc and x is the concentration of DMFc⁺, versus time (s). The slopes of the straight lines represent the apparent rate constants ($k_{\text{app}} / \text{s}^{-1}$) for the reactions with different catalysts (see Table 2).

7 References

- (s1) Partovi-Nia, R.; Su, B.; Li, F.; Gros, C. P.; Barbe, J. M.; Samec, Z.; Girault, H. H. *Chem.--Eur. J.* **2009**, *15*, 2335-2340.
- (s2) Chang, C. J.; Loh, Z. H.; Shi, C.; Anson, F. C.; Nocera, D. G. *J. Am. Chem. Soc.* **2004**, *126*, 10013-10020.
- (s3) Kakiuchi, T.. In *Liquid-liquid interfaces, Theory and methods*; Volkov, A.G., Deamer, D.W., Eds.; CRC Press: Boca Raton, 1996; pp 1-18.
- (s4) Peljo, P.; Rauhala, T.; Murtomäki, L.; Kallio, T.; Kontturi, K. *Int. J. Hydrogen Energy* **2011**, *36*, 10033-10043.
- (s5) Hatay, I.; Su, B.; Li, F.; Méndez, M. A.; Khoury, T.; Gros, C. P.; Barbe, J. M.; Ersoz, M.; Samec, Z.; Girault, H. H. *J. Am. Chem. Soc.* **2009**, *131*, 13453-13459.
- (s6) Girault, H. H. *Analytical and Physical Electrochemistry*; EPFL Press: Lausanne, Switzerland, 2004.
- (s7) Chung, T. D.; Anson, F. C. *Anal. Chem.* **2000**, *73*, 337-342.
- (s8) Stephenson, R. M. *J. Chem. Eng. Data* **1994**, *39*, 225-227.
- (s9) Ge, P.; Scanlon, M. D.; Peljo, P.; Bian, X.; Vubrel, H.; O'Neill, A.; Coleman, J. N.; Hu, X.; Kontturi, K.; Liu, B.; Girault, H. H., submitted, 2012.
- (s10) Atkins, P. W. *Physical Chemistry*; 4th ed.; Oxford University Press: Oxford, 1990.